Second moment of the Husimi distribution as a measure of complexity of quantum states

Ayumu Sugita

Research Center for Nuclear Physics, Osaka University,

10-1 Mihogaoka, Ibaraki, Osaka 567-0047, Japan

Hirokazu Aiba

Kyoto Koka Women's College,

38 Kadono-cho Nishikyogoku,

Ukyo-ku, 615-0882, Japan

(Dated: February 8, 2008)

Abstract

We propose the second moment of the Husimi distribution as a measure of complexity of quantum states. The inverse of this quantity represents the effective volume in phase space occupied by the Husimi distribution, and has a good correspondence with chaoticity of classical system. Its properties are similar to the classical entropy proposed by Wehrl, but it is much easier to calculate numerically. We calculate this quantity in the quartic oscillator model, and show that it works well as a measure of chaoticity of quantum states.

PACS numbers: 05.45.Mt, 05.45.Ac

I. INTRODUCTION

Although the quantum manifestation of chaos has been extensively studied over the past few decades, to define "quantum chaos" is still the main problem in this field. The direct extension of the definition applicable to classical chaos seems to fail because of the linearity of the Schrödinger equation. Since quantum mechanics contains classical mechanics as a limit, however, there must be something in quantum mechanics that produces classical chaos in the classical limit.

There have been many attempts to define a measure of quantum chaos. There are some measures using the level statistics, but much more information could be obtained from analysises of individual quantum states. We can classify measures of complexity of quantum states into two types:

1. complexity of pure states

2. complexity of an ensemble of quantum states

For example, the von Neumann entropy of the density matrix belongs to type (2). In this paper, we focus on complexity of type (1).

Some quantities defined in terms of the expansion coefficients are often used in numerical calculations. For instance, suppose a quantum state is expanded in an appropriate basis $\{|i\rangle\}$:

$$|\varphi\rangle = \sum_i c_i |i\rangle. \tag{1}$$

Let us define $p_i = |c_i|^2$. Then the information (Shannon) entropy

$$S = -\sum_i p_i \ln p_i, \tag{2}$$

and moments of the distribution

$$M_k = \sum_i p_i^k, \tag{3}$$

are measures of localization (or delocalization) with respect to this basis. In particular, the inverse of the second moment M_2^{-1} is called the number of principal components (NPC): it becomes unity when the state has only one component, while it becomes n when the

probability is equally distributed over n basis vectors. Such quantities are easy to calculate. However, an obvious defect is that the definition depends on the basis.

Wehrl has proposed a good measure of complexity of quantum states based on the Husimi distribution function $\rho_H(\boldsymbol{p}, \boldsymbol{q})$ [1][2]. He called it "classical entropy",

$$S(\rho_H) = \int d\boldsymbol{p} d\boldsymbol{q}\ \rho_H \ln \rho_H, \tag{4}$$

while in his paper "quantum entropy" denotes the von Neumann entropy of a density matrix. Note that the classical entropy is applicable and takes various values also for pure states, while the quantum entropy always vanishes for them. Although Wehrl introduced the classical entropy as an approximation to the quantum entropy, their values are not necessarily close even in the limit $\hbar \to 0$. (See the discussion in [4].) According to our classification, we discuss the classical entropy to describe complexity of type (1), i.e. of pure states.

Chaoticity in classical mechanics can be characterized by the delocalization of orbits. In integrable systems, there are many constraints from symmetries, such that orbits are confined to low-dimensional tori. As the system becomes chaotic, the tori are destroyed and orbits can spread to higher dimensional space. In highly chaotic systems, orbits spread uniformly over the equi-energy surface. Such systems are called ergodic. Among the several conditions to characterize chaoticity of classical mechanics, the ergodicity is a rather weak one. For example, any one-dimensional time-independent Hamiltonian system is ergodic, but never chaotic. However, in physically natural situations of many-dimensional systems, the ergodicity works as a definition of classical chaos.

We can expect a similar behavior in quantum mechanics. The Husimi function is a function on phase space, and takes only non-negative values while the Wigner function can be negative and is usually violently oscillating [4]. Hence the Husimi function can be regarded as a probability distribution in phase space, and its order of delocalization can be a measure of chaoticity of quantum states. In that sense, Wehrl's classical entropy seems to be a good candidate measure.

However, Wehrl's entropy is defined as an integral over phase space, and is not easy to calculate numerically. To the best of the authors' knowledge, there is no calculation for a more than one-dimensional system. (A calculation for a one-dimensional time-driven system is in [4].) The difficulty mainly comes from the redundancy of the Husimi function: the Husimi function of k dimensional system is a function on $2k$ dimensional space, while a

function on k dimensional space is enough to keep the same information in either coordinate or momentum representation.

Complex pure quantum states are usually represented as sets of expansion coefficients with respect to a basis. This will be the case also in our following discussion. When we calculate Wehrl's entropy of a quantum state, the normal procedure is the following:

1. Calculate the Husimi function ρ_H on many sampling points $\{(\boldsymbol{p}_i, \boldsymbol{q}_i)\}$.

2. Take an average $\langle \rho_H \ln \rho_H \rangle$ over the sampling points.

However, this procedure seems to be overly excessive because we have all the information about the quantum state in the set of expansion coefficients. There must exists some formula to calculate the average directly from the coefficients. The main concern of this paper is to avoid the redundancy of the Husimi function in numerical evaluation of a suitable measure of complexity. In other words, we wish to know how to get some averages related to the Husimi function without actually calculating the Husimi function itself.

It seems difficult to derive a simple formula for the entropy because of the transcendental logarithmic function. However, a simple formula is possible for an algebraic function. The second moment, which is the average of the square of the distribution function, is especially easy to calculate. We will show later a formula in which the second moment of the Husimi distribution is expressed directly in terms of expansion coefficients in the harmonic oscillator basis. (If the quantum states are given by expansion coefficients in another basis, we should calculate the transformation matrix and change the basis to the harmonic oscillator basis.) The numerical effort is of order N^2 for a quantum state where N is the number of basis vectors. If we calculate the second moments for all quantum states given by diagonalization of a $N \times N$ matrix, the numerical effort is of order N^3, which is the same as the order of the diagonalization of the matrix.

We represent the inverse of the second moment by W_2:

$$W_2(\rho_H) = \frac{1}{M_2(\rho_H)}, \tag{5}$$

$$M_2(\rho_H) = \int \frac{d\boldsymbol{p}d\boldsymbol{q}}{(2\pi\hbar)^k} \, \rho_H(\boldsymbol{p}, \boldsymbol{q})^2. \tag{6}$$

W_2 represents the effective phase space volume occupied by the Husimi function. For example, if ρ_H takes the same value over a region with volume V and takes zero value outside of it, $W_2 = V$. The unit of W_2 is the Planck cell volume.

Next we summarize the main points of this paper. We use the second moment of the Husimi distribution to define complexity of quantum states. It is a measure of delocalization of the Husimi distribution in phase space. It is defined in a base-independent way and has a good correspondence with complexity of classical mechanics. Moreover, we can calculate it directly from expansion coefficients, without calculating the redundant Husimi function. Therefore it is not so difficult to evaluate numerically.

This paper is organized as follows: In section II we summarize the definition and some properties of the Husimi distribution function. In section III we derive the formula to calculate the second moment of the Husimi distribution directly from expansion coefficients in the harmonic oscillator basis. In section IV we introduce a model Hamiltonian and show numerical results which illustrate the meaning of W_2 as a measure of complexity. The final section is devoted to a summary. In appendix we show details of semiclassical calculations of the second moment of the Husimi distribution in integrable and ergodic limits.

II. HUSIMI DISTRIBUTION FUNCTION

In this section, we review some properties of the Husimi function [3]. We restrict ourselves to a one-dimensional system for simplicity, but the generalization to many-dimensional systems is straightforward.

The Husimi function of a quantum state $|\varphi\rangle$ is defined as

$$\rho_{H,\lambda}(p,q) = |\langle z,\lambda|\varphi\rangle|^2. \tag{7}$$

Here, $|z,\lambda\rangle$ is a coherent state defined as an eigenstate for a complex eigenvalue z

$$\hat{a}_\lambda|z,\lambda\rangle = z|z,\lambda\rangle, \tag{8}$$

where $\hat{a}_\lambda$ is an operator with λ as an arbitrary parameter

$$\hat{a}_\lambda = \frac{1}{\sqrt{2\hbar}}\left(\sqrt{\lambda}\hat{q} + i\frac{\hat{p}}{\sqrt{\lambda}}\right). \tag{9}$$

The real and imaginary parts of z are related to the phase space point (p,q) by

$$q = \sqrt{\frac{\hbar}{2\lambda}}(z+\bar{z}), \tag{10}$$

$$p = -i\sqrt{\frac{\lambda\hbar}{2}}(z-\bar{z}). \tag{11}$$

It is not difficult to derive the relation

$$\rho_{H,\lambda}(p,q) = \frac{1}{\pi\hbar}\int dp'dq'\rho_W(p',q') \times \exp\left[-\frac{1}{\hbar}\left\{\lambda(q'-q)^2+\frac{(p'-p)^2}{\lambda}\right\}\right], \tag{12}$$

where ρ_W is the Wigner function

$$\rho_W(p,q) = \int d\eta\langle q-\eta/2|\varphi\rangle\langle\varphi|q+\eta/2\rangle e^{ip\eta/\hbar}. \tag{13}$$

A state $|q\rangle$ represents an eigenstate of the coordinate representation. There we see that the Husimi function is a kind of the coarse-grained Wigner function. The main advantage of the Husimi function is that it is non-negative, as is obvious from the definition (7). Hence the Husimi function can be formally regarded as a probability distribution, whereas the Wigner function can not.

III. SECOND MOMENT OF THE HUSIMI DISTRIBUTION

In this section, we consider the second moment of the Husimi distribution

$$M_2(\rho_H) = \int \frac{dpdq}{2\pi\hbar}\rho_H(p,q)^2, \tag{14}$$

$$= \int \frac{d^2z}{\pi}|\langle z|\varphi\rangle|^4. \tag{15}$$

Here and in the following we omit λ for simplicity.

Suppose the quantum state $|\varphi\rangle$ is represented in the harmonic oscillator basis

$$|\varphi\rangle = \sum_{n=0}^{\infty} c_n|n\rangle, \tag{16}$$

then M_2 can be expanded as

$$M_2(\rho_H) = \sum_{n,n'}\sum_{m,m'}\frac{c_nc_{n'}c_m^*c_m^*}{\sqrt{n!n'!m!m'!}}\int\frac{d^2z}{\pi}e^{-2|z|^2}\bar{z}^{n+n'}z^{m+m'}, \tag{17}$$

$$= \sum_{n,n'}\sum_{m,m'}\frac{c_nc_{n'}c_m^*c_m^*}{\sqrt{n!n'!m!m'!}}\frac{(n+n')!}{2^{n+n'+1}}\delta_{n+n',m+m'}. \tag{18}$$

$$\tag{19}$$

Here, we used the following formulas

$$\langle n|z\rangle = e^{-|z|^2/2}\frac{z^n}{\sqrt{n!}}, \tag{20}$$

and

$$\int \frac{d^2z}{\pi} e^{-|z|^2} \bar{z}^n z^m = n! \delta_{n,m}. \tag{21}$$

As a result, we obtain the formula

$$M_2(\rho_H) \;=\; \frac{1}{2} \sum_{L=0}^{\infty} |B_L|^2, \tag{22}$$

where

$$B_L \;=\; \sum_{j=0}^{L} \sqrt{\frac{L!}{2^L j!(L-j)!}}\, c_j c_{L-j}. \tag{23}$$

Since there is a truncation $n \leq N$ in the expansion (16) in any real calculation, the sum (22) is also finite. The numerical effort is of order N^2 for a quantum state.

The generalization to many-dimensional systems is straightforward. The result is

$$M_2(\rho_H) \;=\; 2^{-k} \sum_{\boldsymbol{L}} \left| B_{\boldsymbol{L}} \right|^2, \tag{24}$$

where k is the dimension of the system and

$$B_{\boldsymbol{L}} \;=\; \sum_{\boldsymbol{j} \leq \boldsymbol{L}} \sqrt{\frac{\boldsymbol{L}!}{2^{|\boldsymbol{L}|} \boldsymbol{j}!\, (\boldsymbol{L}-\boldsymbol{j})!}}\, c_{\boldsymbol{j}} c_{\boldsymbol{L}-\boldsymbol{j}}. \tag{25}$$

Here, $\boldsymbol{L}$ and $\boldsymbol{j}$ are k-dimensional vectors whose components are non-negative integers. The factorial of those vectors means the product of all factorials of the vector components. For example,

$$\boldsymbol{L}! = \prod_{i=1}^{k} L_i!. \tag{26}$$

The absolute value denotes

$$|\boldsymbol{L}| = \sum_{i=1}^{k} L_i, \tag{27}$$

and $\boldsymbol{j} \leq \boldsymbol{L}$ means $j_i \leq L_i$ for $\forall i$.

IV. NUMERICAL RESULTS

A. Model

The model Hamiltonian we are considering here is that of a two-dimensional quartic oscillator

$$H = \frac{1}{2}(p_x^2 + p_y^2) + \frac{1}{2}(x^4 + y^4) - k x^2 y^2, \tag{28}$$

which has been adopted by many authors for the studies of level statistics and wave functions [5]. We put $\hbar = 1$ and regard all quantities as dimensionless.

This model has the simple scaling property,

$$H(\alpha^2 p_x, \alpha^2 p_y, \alpha x, \alpha y) \;=\; \alpha^4 H(p_x, p_y, x, y), \tag{29}$$

which means that the energy of the system does not essentially change the dynamics. However, the parameter k changes the nature of the system. The system is separable and integrable at $k = 0$, and becomes chaotic as k increases. It is unbound for $k > 1$. Meyer [6] has shown that for large k values (≥ 0.4) the classical phase space structure is almost completely chaotic.

This system has a discrete symmetry called C_{4v}: The Hamiltonian is invariant with respect to reflections about x-axis, y-axis and also about the line $x = y$. In this paper we treat only quantum states which are symmetric under all reflections. (This symmetry class is labeled A_1 in [7].)

B. Structure of the classical phase space

Fig.1 shows the Poincaré surfaces of section of this system at $k = 0.0, 0.2, 0.4$, and 0.6. At $k = 0.0$, the phase space is completely occupied by tori. These tori are partially destroyed at $k = 0.2$, and most of them seem to vanish at $k = 0.4$. However, there are still many islands of stability. The two most significant islands are at $x = 0$. These correspond to the stable linear orbits on $x = y$ and $x = -y$. At $k = 0.6$, we can not recognize any structure. In this case, more than 90% of the orbits are unstable according to [6].

C. Diagonalization of the Hamiltonian

We diagonalize the Hamiltonian (28) in the harmonic oscillator basis. The procedure we used is essentially the same as that of Zimmermann *et al.* [8]. The bases belonging to A_1 can be written as

$$|n_x, n_y\rangle_{A_1} = \frac{|n_x, n_y\rangle + |n_y, n_x\rangle}{\sqrt{2(1 + \delta_{n_x,n_y})}}, \tag{30}$$

where n_x and n_y are even non-negative integer and $n_x \geq n_y$. Matrix elements of the Hamiltonian (28) can be calculated analytically, and we obtain eigenenergies and eigenstates

by the diagonalization of this matrix. The truncated Hilbert space is spanned by the basis vectors with $0 \leq n_x + n_y \leq 270$, whose dimension is 4692.

Among the 4692 eigenstates we obtain by the diagonalization, those having very large energies are not reliable because of the truncation error. Since the range of the validity very much depends on the oscillator frequency ω of the harmonic oscillator basis, we should choose ω to optimize the diagonalization. Because of the variational principle, eigenvalues obtained in the restricted Hilbert space are always higher than the real values, and the level density in that space is always smaller than the real one. Therefore the minimization of $\mathrm{tr}H$ (the sum of the eigenvalues) can be a criterion to choose the optimal ω.

We put $\omega = 7.0$, which is chosen roughly to optimize the diagonalization for $k = 0.6$, for all k. The comparison between the obtained level density and the semiclassical one shows that the maximum reliable energy is $E = 800 \sim 1000$.

D. The second moment of the Husimi distribution and the number of principal components

Figs. 2, 3, 4 and 5 show the results of the numerical calculation of the inverse of the second moment (W_2) of the Husimi distribution for $k = 0.0, 0.2, 0.4$ and 0.6. We plotted them for energy eigenstates with $E \leq 600$. In each figure, $1000 \sim 1500$ eigenstates are plotted. It takes about 30 minutes on the NEC SX-5 in Osaka University to calculate the second moments for all (4692) eigenstates.

When we calculate the Husimi distribution, λ in (7) is a free parameter. The simplest choice is to set λ equal to the harmonic oscillator frequency of the basis used for the diagonalization. In this case, we can directly calculate the second moment using the formulas (24) and (25). The results in Figs. 2, 3, 4 and 5 are calculated using the optimized value $\lambda = 7.0$.

We also calculated W_2 for different values of λ. Fig. 6 shows the results for $\lambda = 4.0, 7.0$ and 10.0 at $k = 0.2$. Qualitative features of the figures seem unchanged, at least when λ is not so far from the optimized value. When λ is far from the optimized value, it is hard to obtain reliable results because the number of basis vectors we need to represent the eigenstates is huge.

At $k = 0.0$, the system is separable into two one-dimensional systems. Therefore eigen-

states of the original system can be specified by quantum numbers m_x and m_y, which label eigenstates of the one-dimensional systems.

We can assume $m_x \geq m_y$ without loss of generality in the class A_1. Fig.7 shows the results of a semiclassical calculation based on the torus quantization. (For details of the calculation, see Appendix A 1.) Semiclassical results and full quantum results have a good correspondence, except for the cases where $m_x \sim m_y$ and $m_y \sim 0$. When $m_x \sim m_y$, the assumption (A21) does not seem to apply. When $m_y \sim 0$, the quantum number is too small to use the semiclassical approximation.

In Fig.3, the regular structure of Fig.2 is partially destroyed, but there are still many regular series of eigenstates. The most significant series, which is in the lowest part of the Fig.3, corresponds to the stable diagonal periodic orbits at $x = y$ and $x = -y$. Fig.8 shows an eigenstate in the regular series. There are also some series of regular eigenstates which are excited in the transverse direction to the periodic orbits.

The lowest series in Fig.2 corresponds to the periodic orbits at $x = 0$ and $y = 0$, which are stable at $k = 0.0$. However, these orbits are unstable at $k > 0$, and this series seems to disappear as k increases.

The eigenstates corresponding to the torus with $E_x = E_y$ are in the middle of Fig.2. (See also Fig.7.) As k increases, this torus is quickly destroyed and two stable diagonal orbits are left. Islands of stability around these two orbits become the most significant structure in this system, and the eigenstates localized around these orbits form the lowest series in Fig.3.

At $k = 0.4$, as seen from Fig.4, there are still regular series that correspond to the diagonal orbits and the first excited states in the transverse direction. However, most structures seem to have been destroyed and many eigenstates are near the ergodic limit, as based on the Berry-Voros hypothesis. (See Appendix A 2.)

At $k = 0.6$, no clear structure can be seen in Fig.5, and the values of W_2 go up as a whole. However, the ergodic limit based on the Berry-Voros hypothesis is still not reached, and some eigenstates have much smaller values than the limit.

There may be several reasons for this. One reason we can think of is that the Wigner function in the Berry-Voros hypothesis does not satisfy the pure state condition of the density matrix $\hat{\rho}^2 = \hat{\rho}$. Therefore we might obtain better estimates of W_2 by taking into account the pure state condition by successive iterations. (See chapter 8 in [9].) Another reason,

which seems more important, is that there are weak localization phenomena like *scars* [10]. We found many scarred eigenstates with small W_2 at $k = 0.6$.

At low energies ($E < 50$), W_2 of some eigenstates reach the ergodic limit irrespective of the value of k, but the figures of these wave functions does not seem chaotic. The reason for this is probably that the semiclassical approximation we used here is not good in this region. Our approximation is based on the idea that the local volume occupied by the Husimi distribution is the volume element of the invariant manifold (invariant torus or equi-energy surface) multiplied by the thickness factor of order $\hbar^{l/2}$, where l is the codimension of the manifold. (See Appendix A.) However, this approximation fails when the scale of the invariant manifold is comparable to the Planck constant. For example, in the low energy part of Fig. 2, the ergodic limit line is under the limit based on the torus quantization. There seems no clear distinction between chaotic and regular eigenstates at very low energies.

In Fig. 9, we plotted the NPC at $k = 0.0, 0.2, 0.4$ and 0.6. We can see regular structure in Fig.9 (a). The structure is gradually broken as k increases, and the points are lifted as a whole. In that sense, the behavior of NPC is similar to that of W_2. However, by comparing NPC and W_2 of each eigenstate, we can see that the two quantities are not so similar. For instance, at $k = 0.4$, we can see regular series of eigenstates related to the diagonal orbits in both Fig. 4 and 9 (c). However, the values of the NPC are not so small, and there are many states lower than the series which seem to have no clear structure. Therefore, in general, W_2 seems more reliable than the NPC as a measure of complexity of quantum states. Some eigenstates that have small NPC are related to the scars of the unstable linear orbits at $x = 0$ and $y = 0$. (See Fig. 10.) Importance of these eigenstates in the response function has been reported in [11].

V. SUMMARY

In this paper we proposed the second moment of the Husimi distribution as a definition of complexity of quantum states. Its inverse (we represent it by W_2) shows the effective volume occupied by the Husimi distribution function, and serves as a measure of delocalization in phase space. We calculated it for a quartic oscillator model, and showed that it has a good correspondence with chaoticity of the classical system. We can calculate it directly from expansion coefficients without numerical integration. Therefore the calculation is not so

time-consuming, and there is no numerical error except for that contained in the quantum state itself.

In the integrable case ($k = 0.0$), the values of W_2 have a regular structure. As k increases, the structure is gradually destroyed and the values go up near the ergodic limit line as a whole. At $k = 0.2$ and 0.4, there are many regular series related to stable islands in classical phase space. Even at $k = 0.6$, the values of W_2 of some eigenstates are much lower than the ergodic limit based on the Berry-Voros hypothesis, and they seem to be related to scars of unstable periodic orbits.

To generalize the idea of this paper to many-body systems using generalized coherent states is interesting. It will be reported in the forthcoming paper [14].

Acknowledgments

The authors thank Prof. V. Dmitrašinović and Dr. E. -M. Ilgenfritz for reading the manuscript and making a number of helpful suggestions. They thank also the members of the Nuclear Theory Group at Kyoto University for valuable discussions. The numerical calculations have been done on NEC SX-5 at Research Center for Nuclear Physics (RCNP), Osaka University. A.S. is supported by the center-of-excellence (COE) program at RCNP.

APPENDIX A: SEMICLASSICAL CALCULATIONS

In this appendix we give, for comparison, semiclassical estimates for the second moment M_2.

1. Integrable case ($k = 0$)

In this case, the model Hamiltonian is separable:

$$H(p_x, p_y, x, y) = h(p_x, x) + h(p_y, y), \tag{A1}$$

$$h(p, x) = \frac{1}{2}\left(p^2 + x^4\right). \tag{A2}$$

Therefore, we first derive a semiclassical formula for the Husimi function of eigenstates of (A2). After that, it is easy to construct the semiclassical eigenstates of (A1) taking into account discrete symmetries.

a. One-dimensional problem

The action variable of the one-dimensional system is

$$I = \frac{1}{2\pi}\oint p dx, \tag{A3}$$

$$= \frac{4}{3\pi}(2E)^{3/4}C, \tag{A4}$$

$$C = \int_0^1 \frac{dx}{\sqrt{1-x^4}} = \frac{1}{4\sqrt{2\pi}}\Gamma\left(\frac{1}{4}\right)^2. \tag{A5}$$

The semiclassical eigenvalues are determined by the Bohr-Sommerfeld quantization condition

$$I(E_m) = (2m+1)\pi\hbar, \tag{A6}$$

i.e.

$$E_m = \frac{1}{2}\left(\frac{3\pi}{4C}\right)^{4/3}\left(m+\frac{1}{2}\right)^{4/3}. \tag{A7}$$

The semiclassical Wigner function of the eigenstate is

$$\rho_W(p,q) = \frac{1}{2\pi}\delta\left(I\left(E(p,q)\right) - I(E_m)\right), \tag{A8}$$

and the Husimi function is obtained by Gaussian smearing thereof:

$$\rho_{H,\lambda}(p,q) \tag{A9}$$

$$= \frac{1}{\pi\hbar}\int dp'dq' \exp\left[\frac{-1}{\hbar}\left\{\lambda(q-q')^2 + \frac{(p-p')^2}{\lambda}\right\}\right]\rho_W(p',q'). \tag{A10}$$

By changing coordinates $q \to q/\sqrt{\lambda}, q' \to q'\sqrt{\lambda}, p \to \sqrt{\lambda}p, p' \to \sqrt{\lambda}p'$, this becomes equivalent to using the modified Hamiltonian

$$H = \frac{\lambda}{2}p^2 + \frac{1}{2\lambda^2}q^4, \tag{A11}$$

and putting parameter $\lambda = 1$ in the Gaussian.

In this case, the Husimi function near the equi-energy surface can be written approximately [4]

$$\rho_H(s,\xi) = \frac{2\sqrt{\pi\hbar}}{T|gradH(s)|}\exp\left[-\frac{(\xi-\xi_0)^2}{\hbar}\right]. \tag{A12}$$

Here, s is a coordinate which parameterizes the equi-energy surface. ξ is the other coordinate, and $\xi = \xi_0$ corresponds to a point on the surface. s and ξ are assumed to be orthonormal. T is the period, whose explicit form is

$$T = 4C(2E)^{-1/4}. \tag{A13}$$

To calculate $M_2(\rho_H)$, we introduce new coordinates (E, θ) as

$$p = \sqrt{\frac{2E}{\lambda}} \sin\theta, \tag{A14}$$

$$q = (2E)^{1/4} \sqrt{\lambda} \cos^{1/2}\theta. \tag{A15}$$

Then

$$M_2(\rho_H) = \int \frac{d\xi ds}{2\pi\hbar} \rho_{H,x}(\xi, s)^2, \tag{A16}$$

$$= \frac{\sqrt{2\pi\hbar}}{T^2} \int d\theta \left|\frac{ds}{d\theta}\right| \frac{1}{|gradE(\theta)|^2}, \tag{A17}$$

$$= \frac{1}{32C^2} \sqrt{\frac{2\pi\hbar}{E}} \int_0^{\pi/2} \frac{d\theta}{\sqrt{\frac{1}{\lambda}\cos^4\theta + \frac{\lambda}{4\sqrt{2E}} \sin^2\theta \cos\theta}}. \tag{A18}$$

b. Two-dimensional solutions

Since the model (28) has some discrete symmetries, we have to take them into account when we construct semiclassical eigenstates. For example, in the class A_1, an eigenstate is written as

$$|m_x, m_y\rangle_{A_1} = \frac{|m_x, m_y\rangle + |m_y, m_x\rangle}{\sqrt{2(1+\delta_{m_x,m_y})}}, \tag{A19}$$

where $|m_x, m_y\rangle$ is the product of one-dimensional eigenstate of (A2), and both m_x and m_y are even.

If $m_x \neq m_y$, the Husimi function of the eigenstate is

$$|\langle z|m_x, m_y\rangle_{A_1}|^2 = \frac{1}{2}\left(|\langle z|m_x, m_y\rangle|^2 + |\langle z|m_y, m_x\rangle|^2 + 2\mathrm{Re}\langle m_x, m_y|z\rangle\langle z|m_y, m_x\rangle\right). \tag{A20}$$

In the semiclassical approximation, $|m_x, m_y\rangle$ and $|m_y, m_x\rangle$ correspond to different tori. Therefore we assume

$$\langle m_x, m_y|z\rangle\langle z|m_y, m_x\rangle \sim 0. \tag{A21}$$

Under this assumption,

$$\rho_H(|m_x, m_y\rangle_{A_1}) = \begin{cases} \frac{1}{2}\left(\rho_H(|m_x, m_y\rangle) + \rho_H(|m_y, m_x\rangle)\right) & (m_x \neq m_y) \\ \rho_H(|m_x, m_y\rangle) & (m_x = m_y) \end{cases}. \tag{A22}$$

The second moments are

$$M_2 = \begin{cases} \frac{1}{2} M_2(E_{m_x}) M_2(E_{m_y}) & (m_x \neq m_y) \\ M_2(E_{m_x}) M_2(E_{m_y}) & (m_x = m_y) \end{cases}. \tag{A23}$$

Here, $M_2(E)$ denotes the second moment of the one-dimensional problem at energy E, whose explicit form is given in (A18). E_n is the n-th eigenenergy of the one-dimensional problem, as given in (A7).

If we change E_x and E_y fixing the total energy $E = E_x + E_y$, the product $M_2(E_x)M_2(E_y)$ takes its minimum value at $E_x = E_y$ because $M_2(E)$ behaves like E^α with $-1/2 \leq \alpha \leq -1/4$. Therefore the upper limit of W_2 with fixed E (we denote this as $\bar{W}_2(E)$) is

$$\bar{W}_2(E) = \frac{2}{M_2\left(\frac{E}{2}\right)^2}. \tag{A24}$$

W_2 of the eigenstates with $m_x \sim m_y$ are close to $\bar{W}_2$, but if $m_x = m_y$, W_2 of the state is one half of $\bar{W}_2$.

2. Ergodic limit

In this subsection, we calculate the Husimi distribution corresponding to the Berry-Voros hypothesis [12, 13] and the second moment thereof.

The Berry-Voros conjecture can be stated as saying that the Wigner function for the stationary state of an ergodic system is approximately

$$\rho_W(\boldsymbol{p}, \boldsymbol{q}) = N_W \delta\{E - H(\boldsymbol{p}, \boldsymbol{q})\}, \tag{A25}$$

where the normalization is, in k dimensions,

$$N_W = \left[\int \frac{d\boldsymbol{p} d\boldsymbol{q}}{(2\pi\hbar)^k} \delta\{E - H(\boldsymbol{p}, \boldsymbol{q})\}\right]^{-1}. \tag{A26}$$

The Husimi function $\rho_{H,\lambda}$ is obtained by smearing (A25) by the Gaussian $e^{-\lambda \boldsymbol{q}^2 - \boldsymbol{p}^2/\lambda}$. From the discussion in the previous section, we can see that this is equivalent to using the modified Hamiltonian

$$H = \frac{\lambda}{2}(p_x^2 + p_y^2) + \frac{1}{2\lambda^2}(x^4 + y^4) - \frac{k}{\lambda^2} x^2 y^2, \tag{A27}$$

and putting $\lambda = 1$ in the Gaussian.

We use coordinates $(E, \theta_1, \theta_2, \theta_3)$, which are related to original coordinates by the following equations:

$$p_x = \sqrt{\frac{2E}{\lambda}} \cos\theta_1 \cos\theta_2, \tag{A28}$$

$$p_y = \sqrt{\frac{2E}{\lambda}} \cos\theta_1 \sin\theta_2, \tag{A29}$$

$$x = \frac{E^{1/4}\sqrt{\lambda}}{f(\theta_3)} \sin^{1/2}\theta_1 \cos\theta_3, \tag{A30}$$

$$y = \frac{E^{1/4}\sqrt{\lambda}}{f(\theta_3)} \sin^{1/2}\theta_1 \sin\theta_3, \tag{A31}$$

where

$$f(\theta) = \left\{ \frac{1}{2}(\cos^4\theta + \sin^4\theta) - k\cos^2\theta\sin^2\theta \right\}^{1/4}. \tag{A32}$$

The normalization constant of the Wigner function N_W is determined as

$$N_W^{-1} = \int \frac{d\boldsymbol{p}d\boldsymbol{q}}{(2\pi\hbar)^2} \delta(E - H(\boldsymbol{p}, \boldsymbol{q})), \tag{A33}$$

$$= \frac{4\pi\sqrt{E}}{(2\pi\hbar)^2} \int_0^{\pi/2} \frac{d\theta}{f(\theta)^2}, \tag{A34}$$

$$= \frac{\sqrt{2E}}{\pi\hbar^2} K\left(\sqrt{\frac{1+k}{2}}\right). \tag{A35}$$

Here, K is the complete elliptic integral. The Husimi function in this case is

$$\rho_H(\boldsymbol{p}, \boldsymbol{q}) = \frac{N_H}{|gradH(\boldsymbol{\sigma})|} \exp\left[\frac{-1}{\hbar}(\xi - \xi_0)^2\right], \tag{A36}$$

where $N_H = N_W/\sqrt{\pi\hbar}$ is the normalization constant. $\boldsymbol{\sigma}$ is the coordinate which parameterizes the equi-energy surface, and $\boldsymbol{\sigma}$ and ξ are orthonormal coordinates. The second moment of ρ_H is

$$M_2(\rho_H) = \int \frac{d\xi d\boldsymbol{\sigma}}{(2\pi\hbar)^2} \rho_H(\xi, \boldsymbol{\sigma})^2, \tag{A37}$$

$$= \frac{N_H^2}{(2\pi\hbar)^2} \sqrt{\frac{\pi\hbar}{2}} \int \left|\frac{\partial\boldsymbol{\sigma}}{\partial\boldsymbol{\theta}}\right| \frac{d\boldsymbol{\theta}}{|gradH(\boldsymbol{\theta})|^2}. \tag{A38}$$

$$\tag{A39}$$

Here,

$$|gradH(\boldsymbol{\theta})|^2 = 2E\cos^2\theta_1 + \frac{4E^{3/2}}{f(\theta_3)^6} \sin^3\theta_1 \left\{\cos^6\theta_3 + \sin^6\theta_3 + K(K-2)\cos^2\theta_3\sin^2\theta\right\}, \tag{A40}$$

and $\left|\frac{\partial \boldsymbol{\sigma}}{\partial \boldsymbol{\theta}}\right| d\boldsymbol{\theta}$ is the volume of a small three-dimensional region formed by $(d\theta_1, d\theta_2, d\theta_3)$. After lengthy, but straightforward calculation we obtain

$$\left|\frac{\partial \boldsymbol{\sigma}}{\partial \boldsymbol{\theta}}\right| = \frac{E^2}{2f(\theta_3)^2}\cos^4\theta_1 + \frac{4E^5}{f(\theta_3)^4}\cos^2\theta_1\sin^2\theta_1\left\{f'(\theta_3)^2 + f(\theta_3)^2\right\}. \tag{A41}$$

Finally we obtain the following formula

$$M_2(\rho_H) \;=\; \frac{N_H^2\pi\sqrt{E}}{2(2\pi\hbar)^{3/2}}\int_0^{2\pi} d\theta_3 \int_0^{\pi/2} \frac{\cos\theta_1 d\theta_1}{f(\theta_3)^2\sqrt{2\lambda E\cos^2\theta_1 + \frac{4E^{3/2}}{\lambda}g(\theta_3)\sin^3\theta_1}}, \tag{A42}$$

where

$$g(\theta) \;=\; \frac{\cos^6\theta + \sin^6\theta + k(k-2)\cos^2\theta\sin^2\theta}{f(\theta)^6}. \tag{A43}$$

---

[1] A. Wehrl, Reps. Math. Phys. **16**, 353 (1979).

[2] A. Wehrl, Rev. Mod. Phys. **50**, 22 (1978).

[3] K. Husimi, Proc. Phys. Math. Soc. Japan, **22**, 246 (1940).

[4] K. Takahashi, Suppl. Prog. Theor. Phys. **98**, 109 (1989).

[5] O. Bohigas, S. Tomsovic and D. Ullmo, Phys. Rep. **51**, 43 (1993).

[6] H. -D. Meyer, J. Chem. Phys. **84**, 3147 (1986).

[7] B. Eckhardt, G. Hose and E. Pollak, Phys. Rev. **A 39**,3776 (1989).

[8] Th. Zimmermann, H.-D. Meyer, H. Köppel and L. S. Cederbaum, Phys. Rev. **A 33**, 4334 (1986).

[9] A. M. Ozorio de Almeida, "Hamiltonian Systems: Chaos and Quantization", Cambridge University Press (1988).

[10] E. J. Heller, Phys. Rev. Lett. **53**, 1515 (1984); Lec. Note in Phys. **263**, 162 (1986).

[11] H. Aiba and T. Suzuki, Phys. Rev. **E63**, 026207 (2001).

[12] M. V. Berry, J. Phys. **A 10**, 2083 (1977).

[13] In "Stochastic Behavior in Classical and Quantum Hamiltonian Systems" (Lecture Notes in Physics 93), ed. G. Casati and J. Ford. New York: Springer, 326.

[14] A. Sugita, in progress.

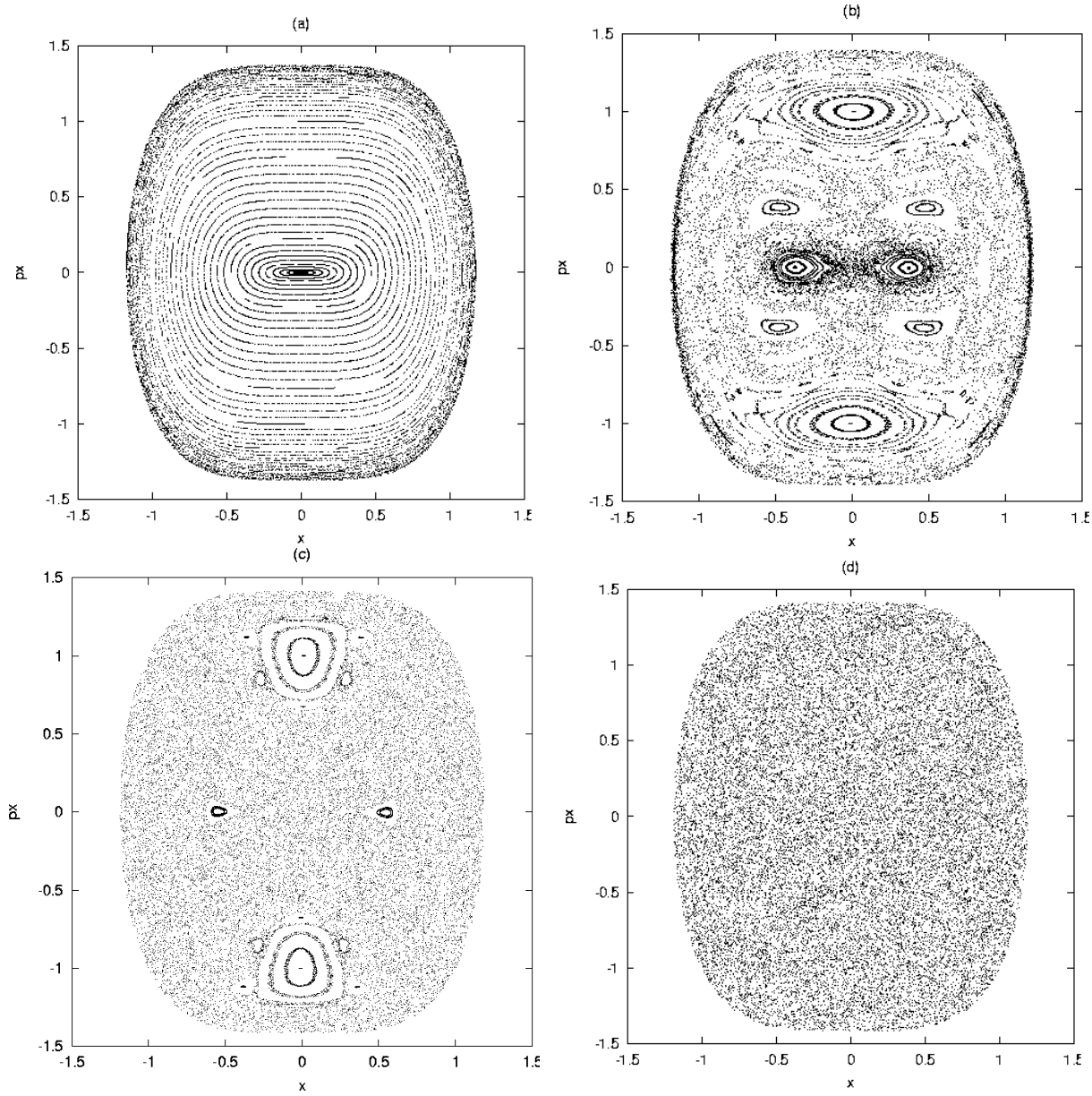

FIG. 1: Poincaré surface of section at $E = 1$ and $y = 0$ for $k = 0.0$ (a), 0.2 (b), 0.4 (c) and 0.6 (d).

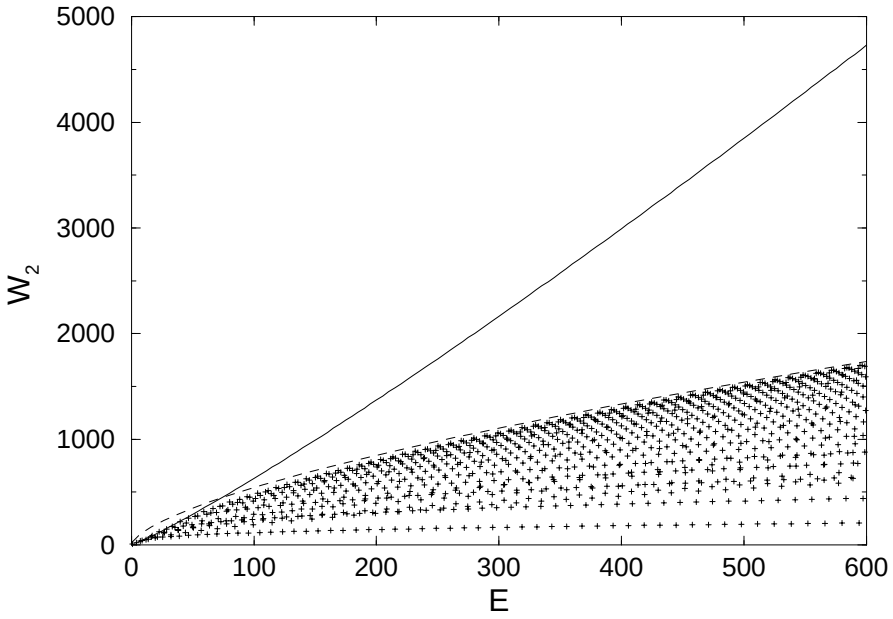

FIG. 2: Results of numerical calculation of W_2 at $k = 0.0$. The solid line shows the ergodic limit calculated based on the Berry-Voros hypothesis. The broken line shows the semiclassical upper limit based on the torus quantization. See Appendix A.

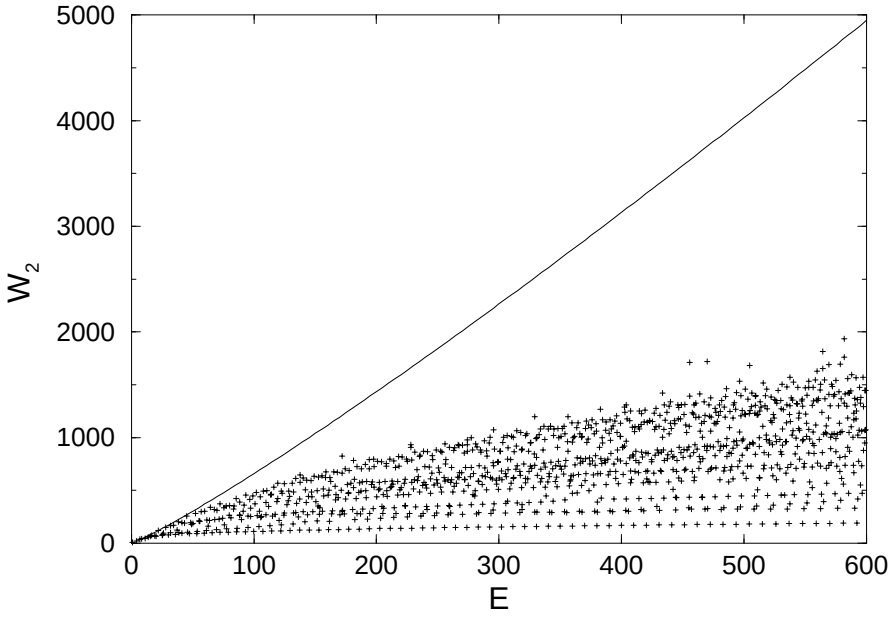

FIG. 3: W_2 at $k = 0.2$.

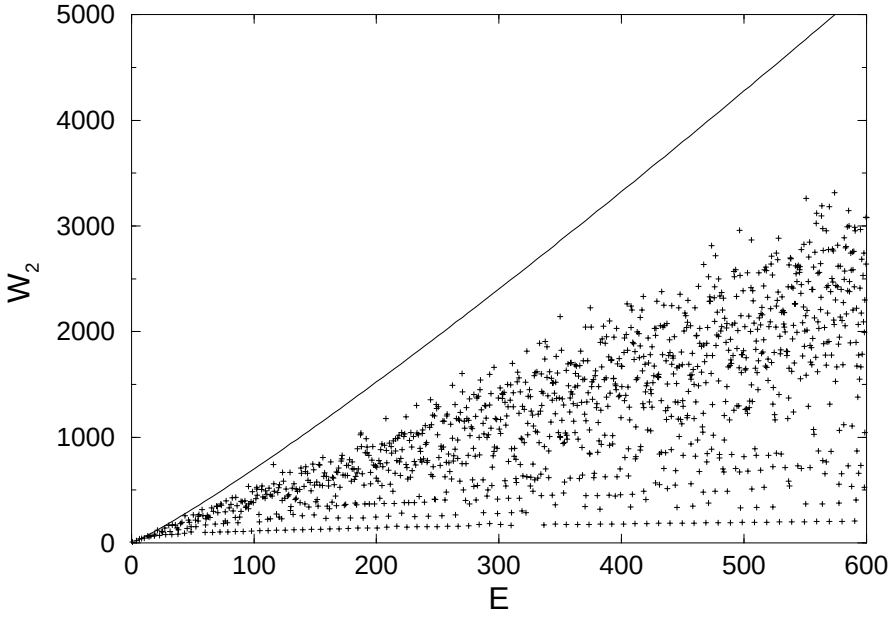

FIG. 4: W_2 at $k = 0.4$.

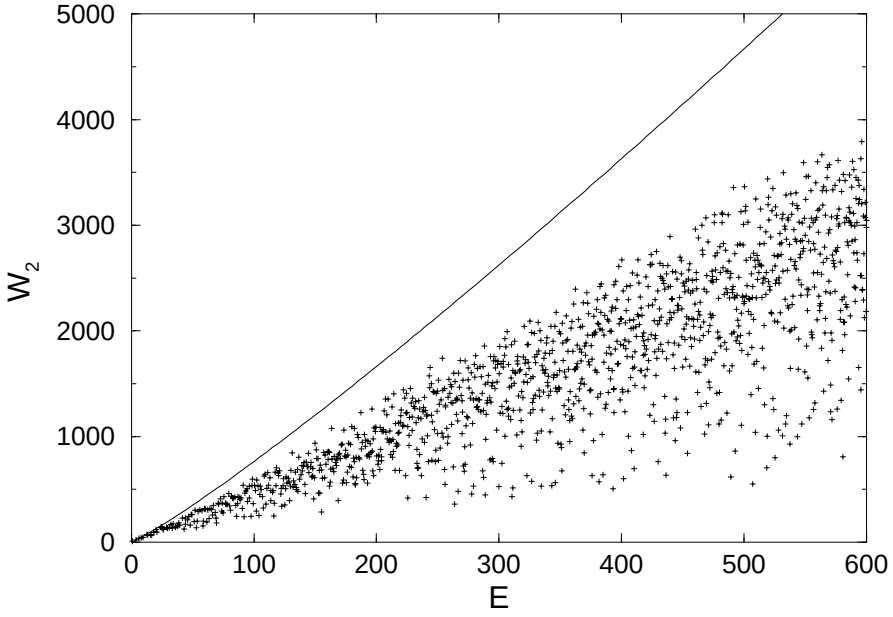

FIG. 5: W_2 at $k = 0.6$.

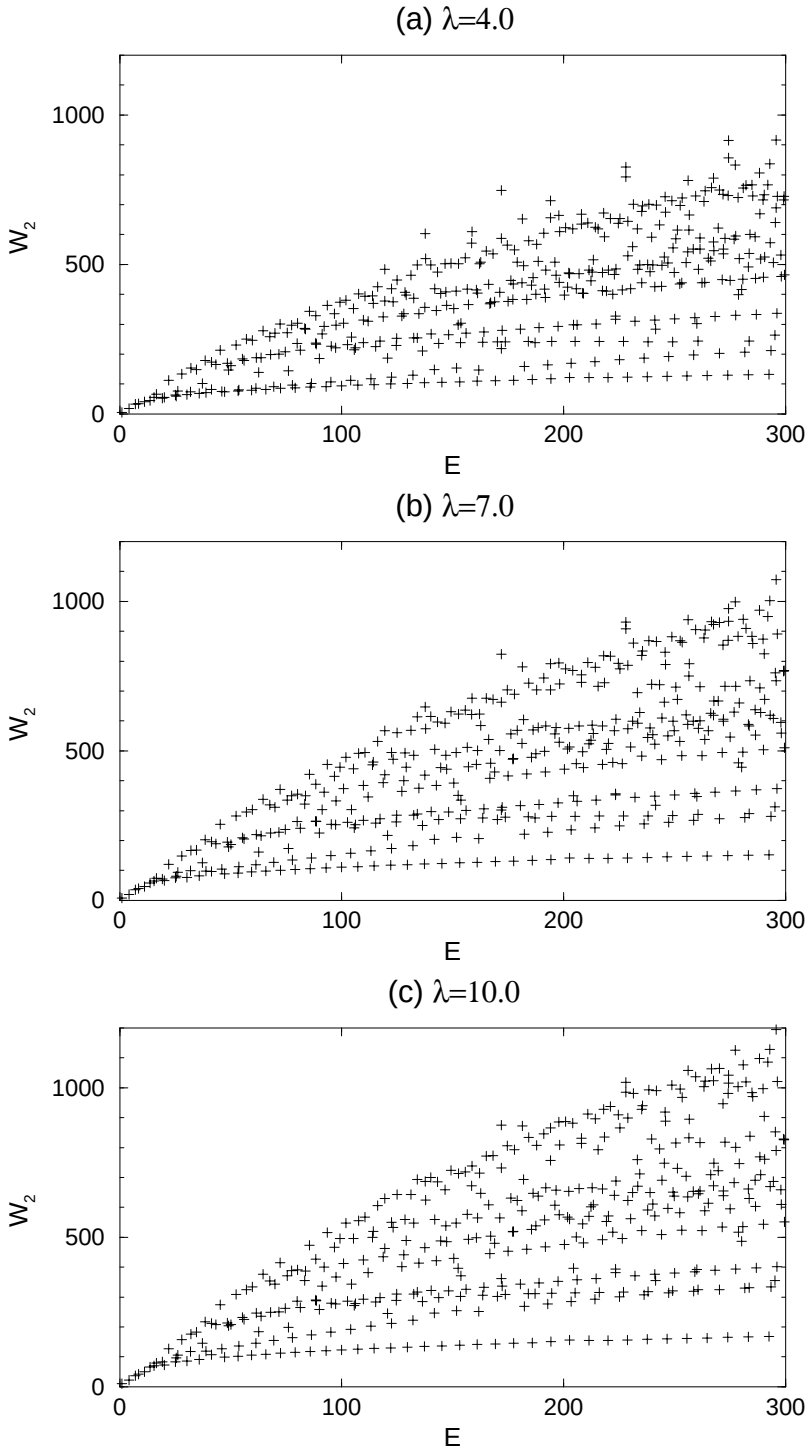

FIG. 6: W_2 at $k = 0.2$ for $\lambda = 4.0$ (a), 7.0 (b) and 10.0 (c). The values of W_2 depend on λ, but the qualitative features remain unchanged.

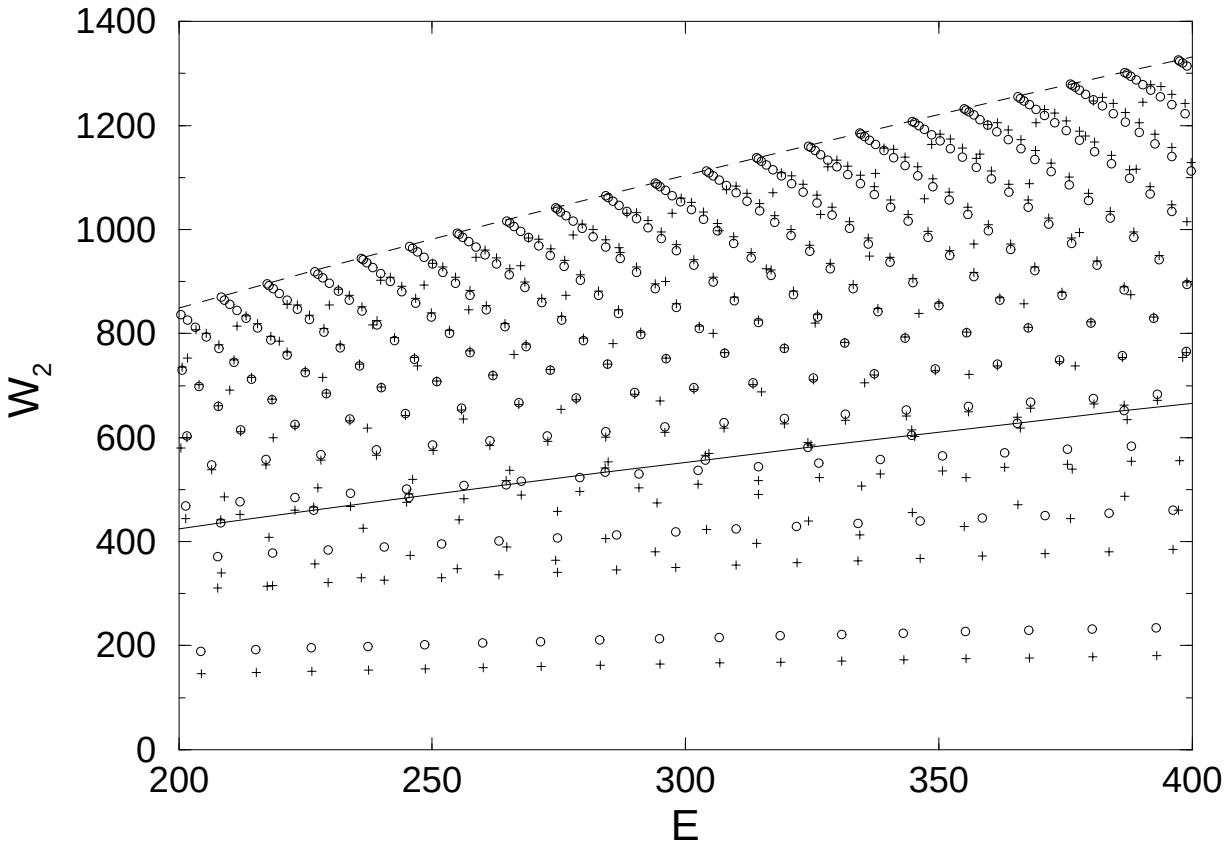

FIG. 7: Comparison between quantum results and semiclassical results based on torus quantization at $k = 0.0$. Pluses are the quantum results and circles are the semiclassical results. The broken line is the upper limit (A24), and the solid line is exactly one half thereof. Eigenstates with $m_x = m_y$ are located on the solid line. In the upper half of this figure, pluses and circles have a good correspondence. However, very near the broken line, the correspondence is lost because the assumption (A21) is not good when $m_x \sim m_y$. In the lower part of this figure, there are eigenstates with small m_y, and semiclassical values are a little higher than the exact values.

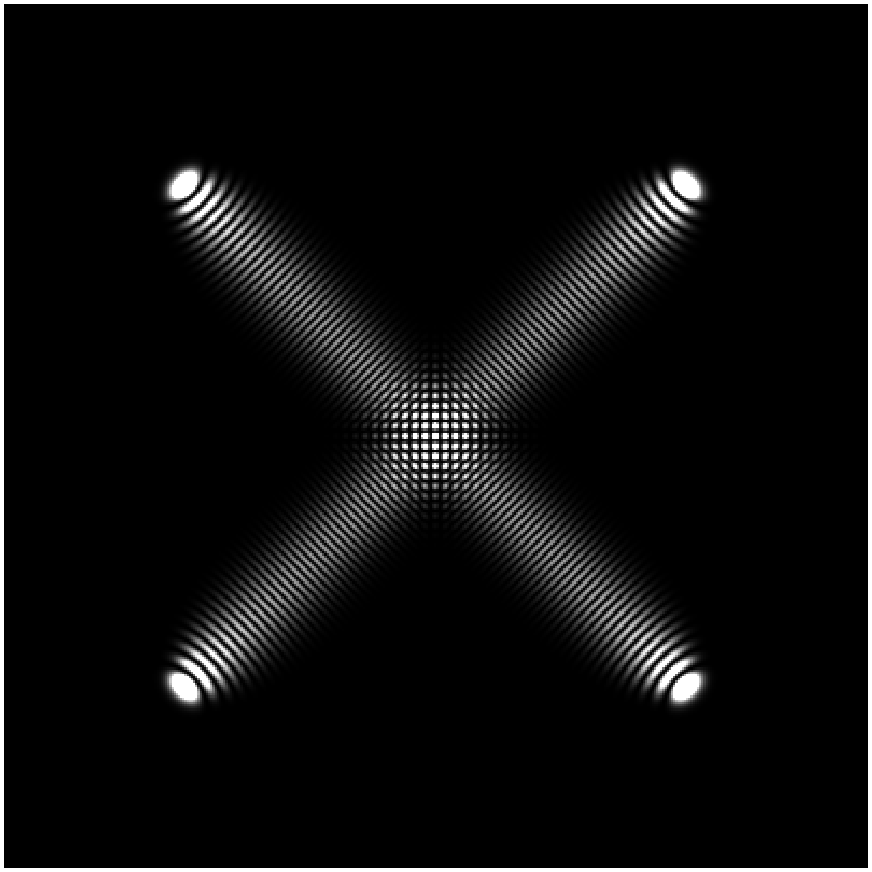

FIG. 8: The density plot of the square of the 441st eigenfunction at k=0.2. E=320.8, W_2=157.2, NPC=102.8. The length of the sides of this figure is 15. This state is completely localized around the diagonal orbits, and there is no node in the transverse direction.

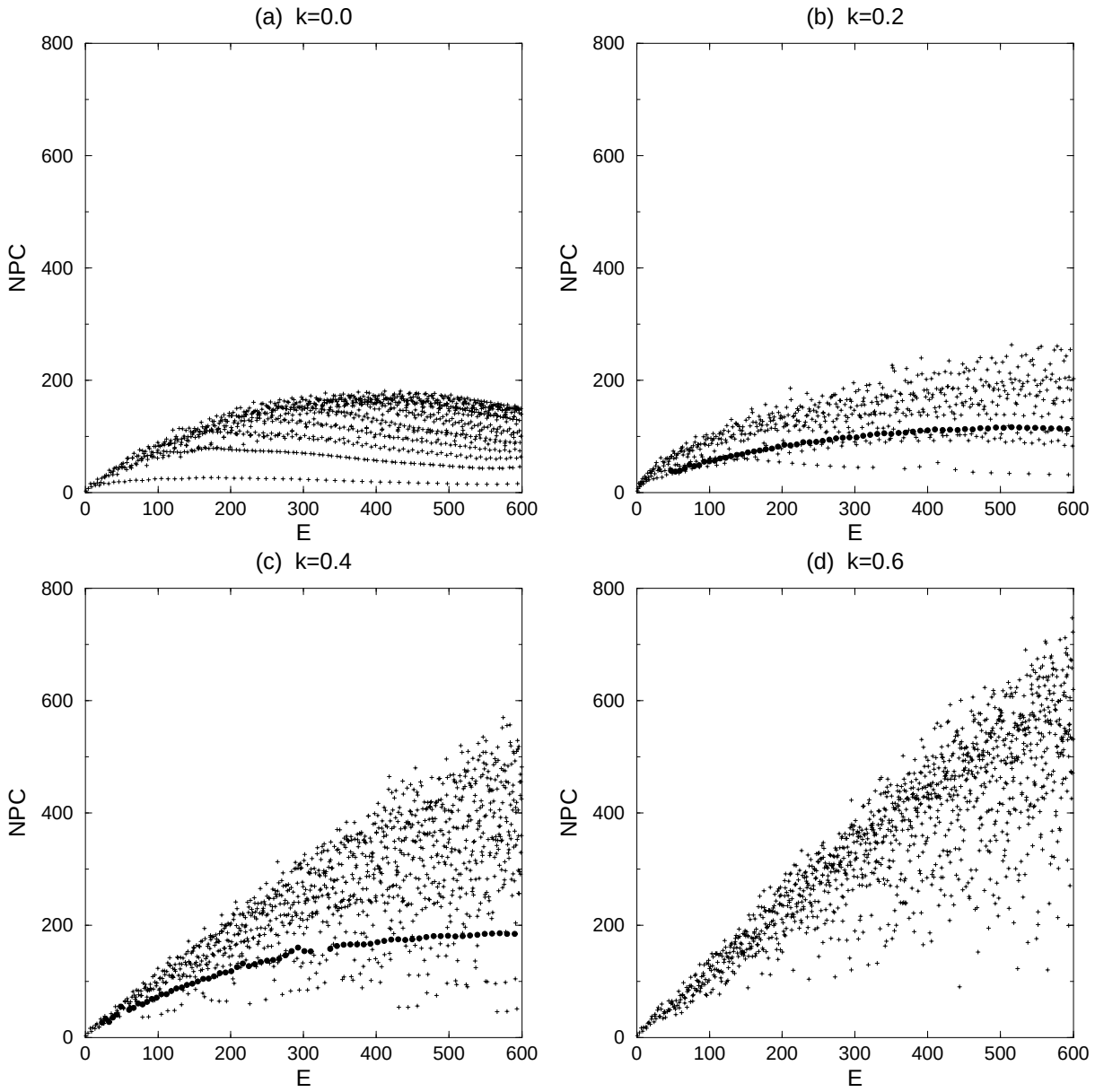

FIG. 9: NPC at $k = 0.0$ (a), 0.2 (b), 0.4 (c) and 0.6 (d). Dots in (b) and (c) show the regular series corresponding to the diagonal orbits.

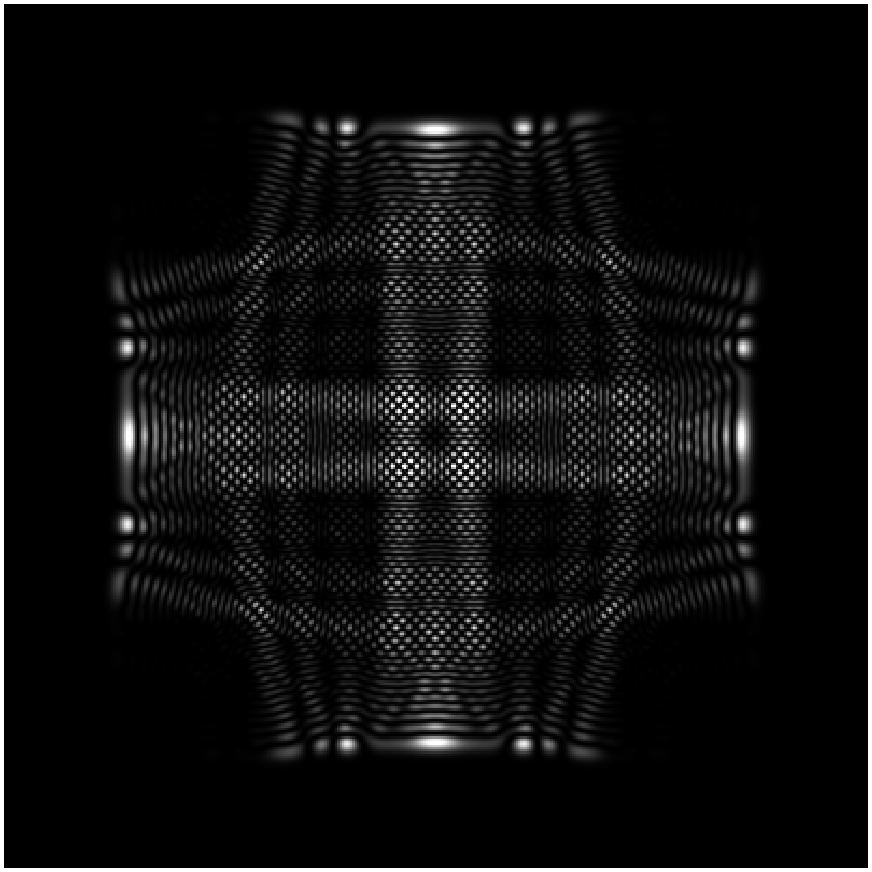

FIG. 10: 754th eigenstate at k=0.4. E=443.6, W_2=545.1, NPC=54.1. NPC of this state is very small, though W_2 is not so small and its structure is not so clear. We can see scars of linear orbits at $x = 0$ and $y = 0$.